SITE EFFECTS MEASURED AT THE NEES@UCSB WILDLIFE STATION FROM THE 2010 OCOTILLO SWARM

Daniel A. Huthsing
Earth Research Institute
UCSB
Santa Barbara, CA 93106
USA

Sandra W. H. Seale
Earth Research Institute
UCSB
Santa Barbara, CA 93106
USA

Jamison H. Steidl
Earth Research Institute
UCSB
Santa Barbara, CA 93106
USA

ABSTRACT

The largest aftershock of the 4 April 2010 M7.2 El Mayor-Cucapah earthquake was a M5.7 event that occurred near Ocotillo, CA, on 15 June 2010. The NEES@UCSB Wildlife Station is a permanently instrumented borehole array located 57km northeast of Ocotillo. Over a period of three months, 60 aftershocks with M > 3.0 were recorded at Wildlife with good signal-to-noise ratio. This data set presented a unique opportunity to study site effects, as the events were co-located with respect to the site and they all have similar focal mechanisms.

In this paper we present spectral ratios for surface-to-downhole signals on all three components. The spectral ratios show clear amplification of the signal at frequencies of engineering interest (< 40 Hz). The east and the north components also have different transfer functions, which suggest anisotropy or a deviation from 1-D layered medium response. We also present spectral ratios of signals recorded in two adjacent boreholes of 5.5m depth, where one borehole has a standard casing and the other has a flexible PVC casing. Our analysis shows that within two standard deviations, the influence of the casing material on the horizontal components of motion is not significant. The vertical component of motion appears to be slightly influenced by the casing material, potentially due to the effect of tube waves.

INTRODUCTION – THE WILDLIFE LIQUEFACTION ARRAY

Borehole arrays of accelerometers have long been a standard tool for monitoring site response and studying the effect of surface geology on strong ground motion. The data collected from borehole arrays have also been used to test and validate models that determine amplification factors for various site categories that are used in seismic hazard mapping. Boreholes can reach depths of hundreds of meters spanning several soil layers. To maintain access to the accelerometers, the boreholes are typically cased with rigid PVC pipe or steel casing.

The Wildlife Liquefaction Array is located on the west bank of the Alamo River, 13 km north of Brawley, California and 160 km east of San Diego. The site is located in the Imperial Wildlife Management Area (Figure 1), a California State game refuge. It was originally instrumented by the USGS in 1982. This region has frequently experienced strong earthquakes: six earthquakes in the past 75 years have induced liquefaction within 10 km of the WLA site (Youd *et al.*, 2007). Based on this history, there is high expectation that additional liquefaction-inducing earthquakes will shake the WLA site in the future.

In 2004, the instrumentation at the WLA site was upgraded by the NSF NEES program. The extensive instrumentation now includes 4 surface accelerometers, 6 downhole accelerometers, 11 sub-surface pore pressure transducers, and numerous benchmarks and inclinometer casings for monitoring lateral ground displacements (Figure 2). The Wildlife site has a liquefiable layer of saturated silty sand, from 2.5m – 6.8m, with silty clay above and below that layer. There are pore pressure transducers at 7 depths within the liquefiable layer and the layer is bracketed with accelerometers at 2.5m and 7.7m depths. Within the layer there are also two accelerometers at 5.5m. The WLA site has state-of-the-art wireless communications systems and operates exclusively on solar power.

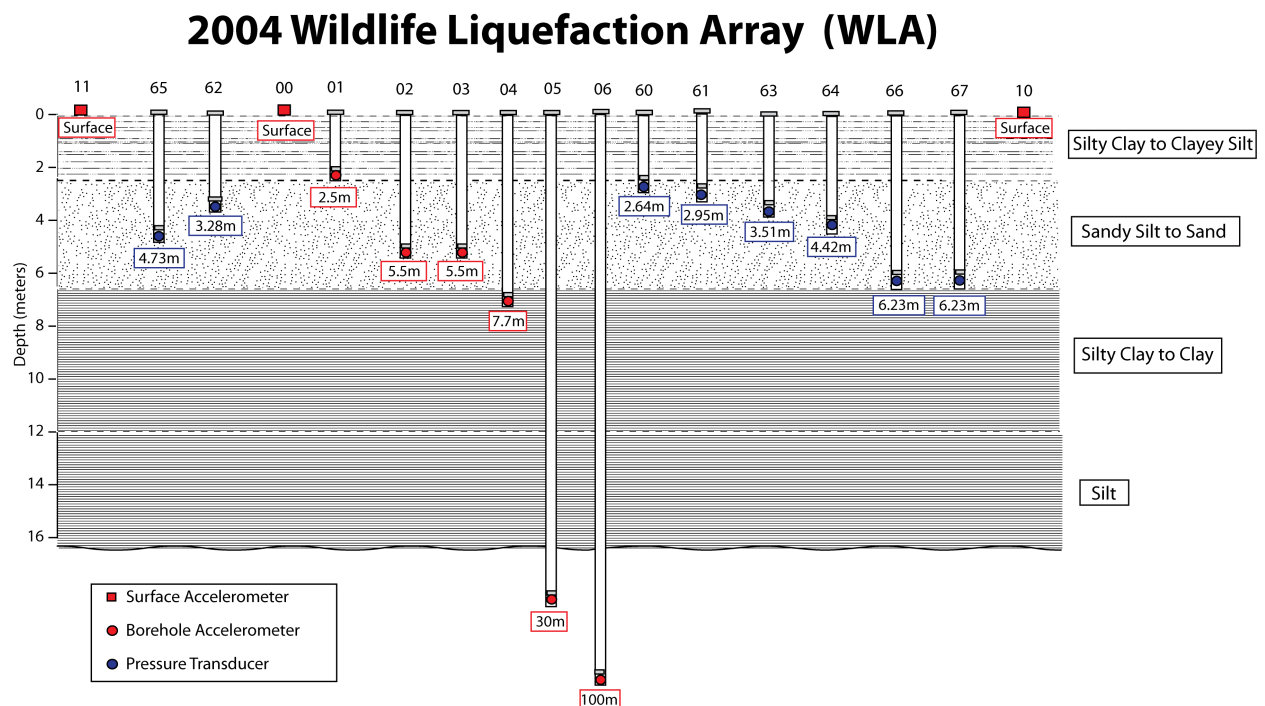*Figure 1. Locations of WLA and UCSB in California.*

Figure 2. Cross-section and instrumentation at WLA.

THE CASING EXPERIMENT

The re-instrumentation of WLA in 2004 offered an opportunity to test the influence of casing material on data recorded by borehole accelerometers. The experiment consists of three accelerometers at WLA, one on the surface and two at depth of 5.5m within the liquefiable layer at WLA. The surface accelerometer is a Kinemetrics EpiSensor FBA ES-T and the two downhole accelerometers are Kinemetrics Shallow Borehole EpiSensors (SBEPI) (nees.ucsb.edu). All three accelerometers are 3-component instruments and are oriented to true north. To test the effect of casing material on the recorded data, one of the sensors at 5.5m is cased in flexible 4" diameter Corex® drain pipe. The other sensor at 5.5m is cased in standard 4" diameter rigid PVC pipe. The goal of this experiment is to determine if there is a difference in the recordings of the two accelerometers which is significant enough to suggest that the data collected by accelerometers in conventional rigid PVC casings may in some way be contaminated by the presence of the PVC casing.

THE DATA

This study examines earthquake data recorded by the accelerometers at WLA. The earthquake data were recorded from 60 aftershocks of the M5.7 event on 14 June 2010 7.7 km ESE of Ocotillo, CA. The M5.7 Ocotillo event is the largest aftershock to date of the M7.2 El Mayor-Cucapah event on 4 April 2010. The surface acceleration recordings of the M5.7 Ocotillo event at WLA are shown below in Figure 3. Accelerations recorded from the larges aftershock (M4.6) are shown in Figure 4.
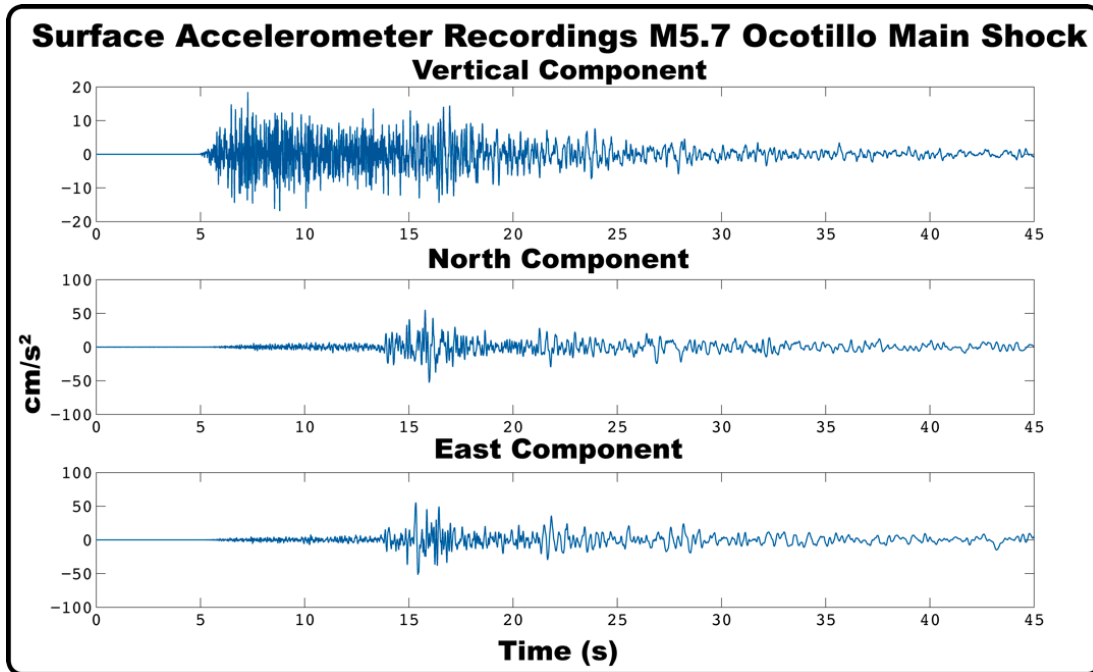

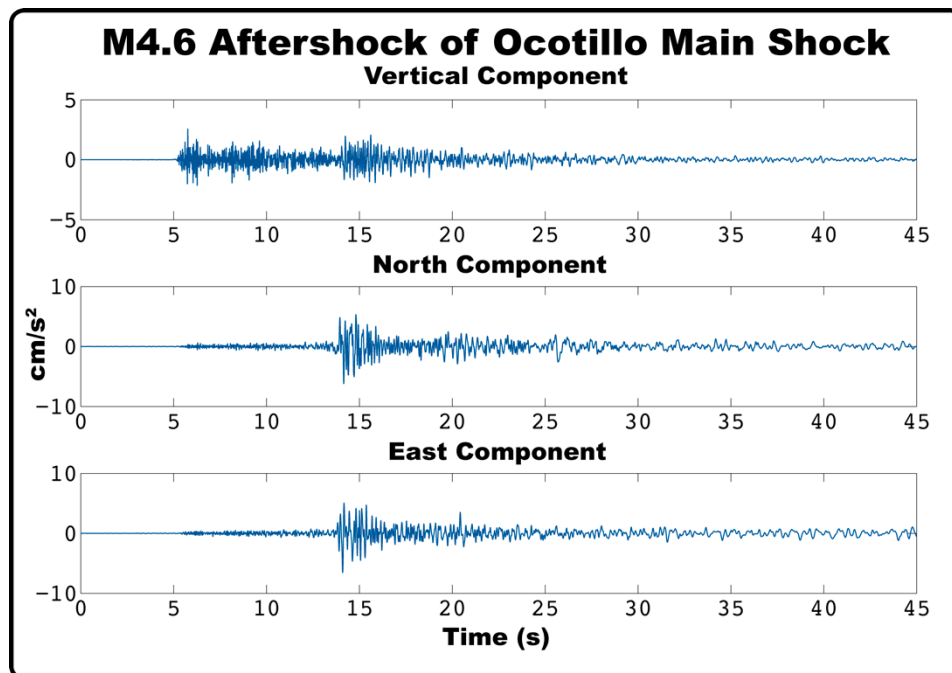*Figure 3. Surface accelerations recorded at WLA from the M5.7 Ocotillo event 14 June 2010.*

Figure 4. Surface accelerations recorded at WLA from the largest aftershock M4.6.
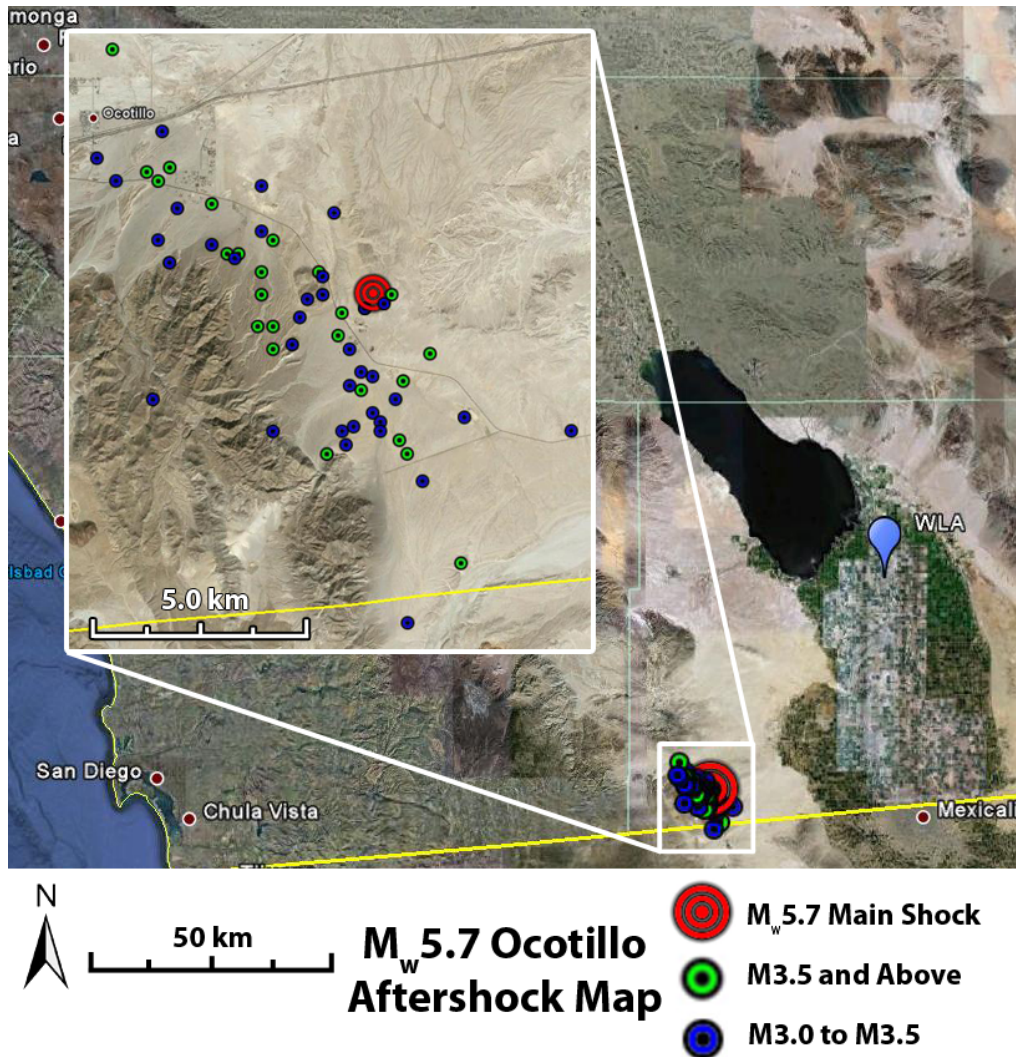
Figure 5. Location of 60 aftershocks of the M5.7 Ocotillo event on 14 June 2010.

This data set consists of 25 events from M3.5 to M4.6 inclusive and 35 events from M3.0 to M3.5. This is swarm of earthquakes presents a unique opportunity to study site effects because it is located relatively close to WLA. Figure 5 above shows the locations of the 60 aftershocks and the M5.7 Ocotillo event.

Table 1 at the end of this paper is a complete list of the events with location, magnitude and distance from WLA.

The data from these sensors were recorded at 200 Hz by 6-channel 24-bit Quanterra Q330 data loggers and streamed to UCSB in real-time using the High Performance Wireless Research and Education Network (HPWREN). The data were stored, processed and made available to the public through the NEES@UCSB website http://nees.ucsb.edu/.

ANALYSIS

For each event, a Discrete Fourier Transform for every component of each sensor was computed using Matlab's Fast Fourier Transform (FFT) algorithm. Each FFT was then smoothed with a 1% running window. The events were then sorted by magnitude into three groups: the main shock, events of magnitude M4.6 thru M3.5 and events of magnitude M3.5 to M3.0. The spectral amplitudes of the signals were then averaged together in each group. Figure 6 below shows the average spectral amplitudes for the three groups of events. The red line is the spectrum of the Mw5.7 main shock. The green line is an average of the spectra of 25 aftershocks with magnitudes greater than 3.5 (for the east component 21 spectra were averaged). The blue line is an average of the spectra of 35 aftershocks with magnitudes between 3.0 and 3.5 (for the east component 29 spectra were averaged). The similar shape of these spectra shows the consistency of source mechanism between the three sets of events.
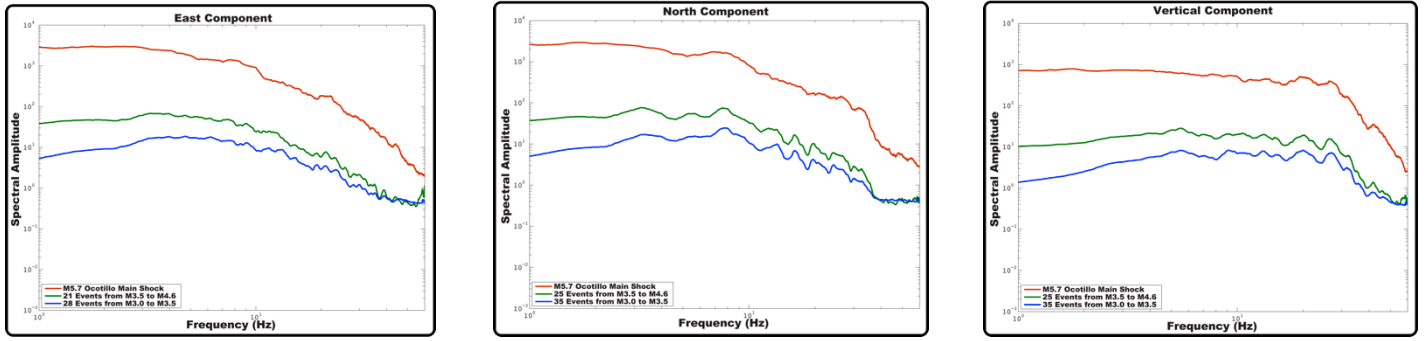
Figure 6. The frequency spectra of the three components of motion for the surface accelerometer at WLA. The red line is the spectrum of the Mw5.7 main shock. The green line is an average of the spectra of 25 aftershocks with magnitudes greater than 3.5 (for the east component 21 spectra were averaged). The blue line is an average of the spectra of 35 aftershocks with magnitudes between 3.0 and 3.5 (for the east component 29 spectra were averaged). The similar shape of these spectra shows the consistency of source mechanism between the three sets of events.

Downhole to Surface Transfer Functions

The average frequency spectra were also computed for the accelerometers at 30m and 100m depths. Dividing the average surface spectrum by the spectrum at depth results in a transfer function. Peaks in the transfer function can be resonant frequencies of the surface layers or they can be the result of destructive interference of downgoing seismic waves.

Figures 7 – 9 below show the transfer functions for the east, north and vertical components at 30m and 100m. Again, the results are presented by groups of event magnitude, where the red line is the M5.7 main shock, the green line is the 21 events from M3.5 to M4.6 and the blue line is the 28 events from M3.0 to M3.5. The transfer function from the 30m depth is on the left, the transfer function for the 100m depth is on the right.
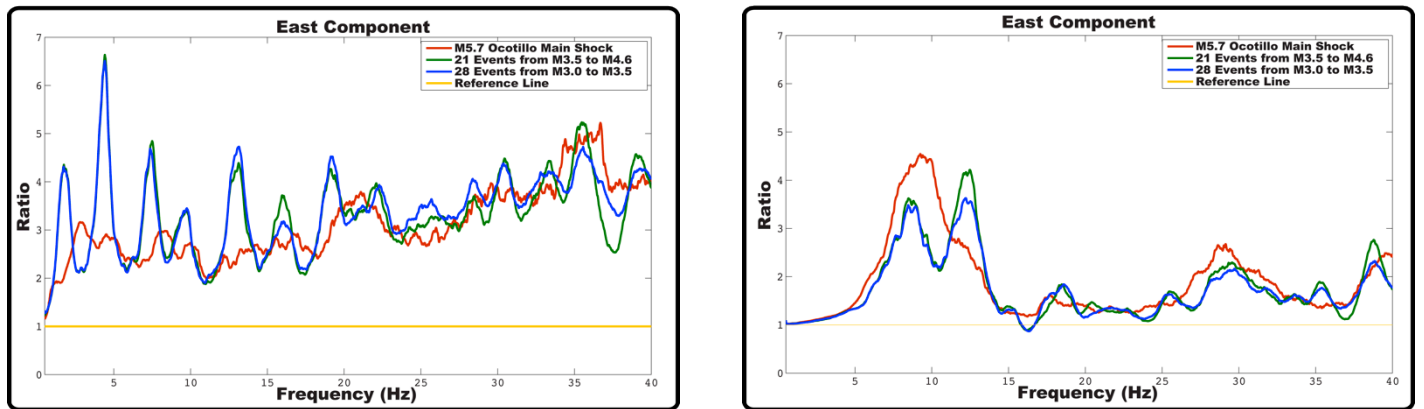

Figure 7. Transfer functions for the east component at WLA from accelerations recorded from the M5.7 Ocotillo event and the swarm of aftershocks. The results are presented by groups of event magnitude, where the red line is the M5.7 main shock, the green line is the 21 events from M3.5 to M4.6 and the blue line is the 28 events from M3.0 to M3.5. The transfer function from the 30m depth is on the left, the transfer function for the 100m depth is on the right.

Several features of these data can be seen. It is notable that the two groups of aftershocks have almost identical transfer functions. It is reassuring that the data set is robust for this analysis. For the east and north components, more peaks are visible from the 30m transfer function than the 100m transfer function. This is primarily due to destructive interference of downgoing waves that have not attenuated enough at 30m but are no longer seen at 100m depth. It is also notable that the peaks on the east and north components occur at different frequencies, indicating possible anisotropy in the surface material at WLA. For the vertical component, the peaks in the transfer functions of the smaller events closely match the peaks in the transfer function of the M5.7 Ocotillo event. The difference between the mainshock and aftershock response are indications that nonlinear soil behavior may be starting to be a factor.
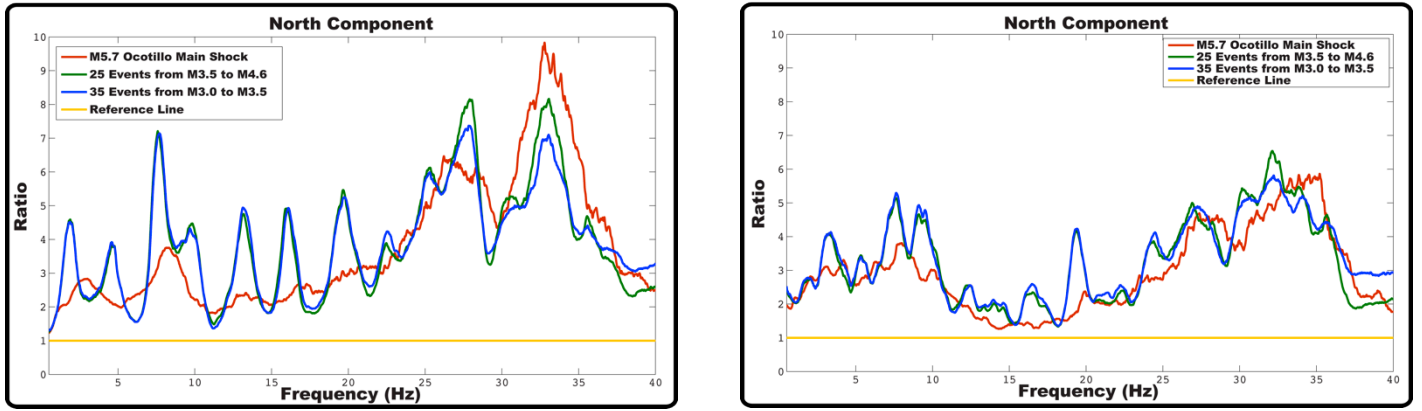
Figure 8. Transfer functions for the north component at WLA from accelerations recorded from the M5.7 Ocotillo event and the swarm of aftershocks.
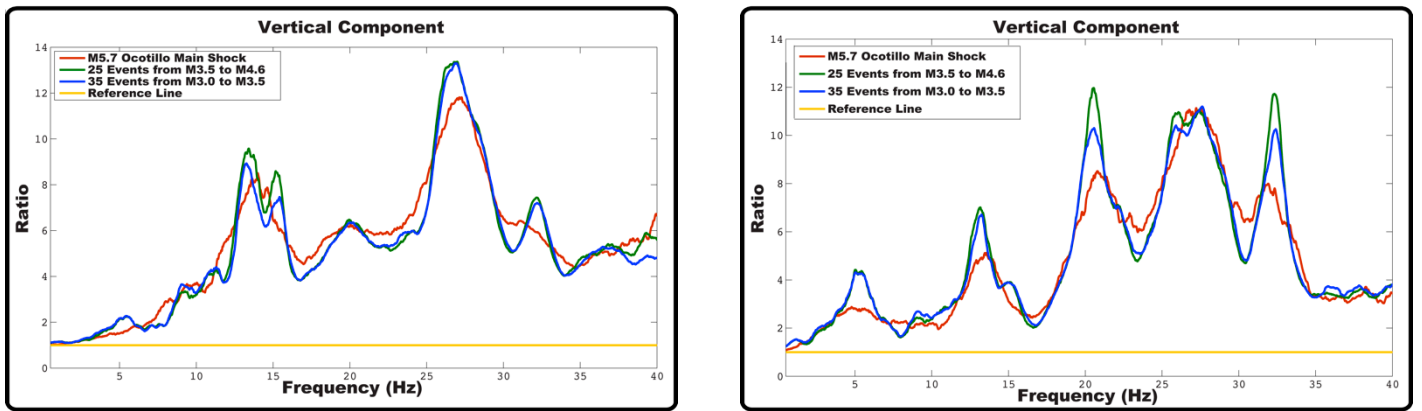

Figure 9. Transfer functions for the vertical component at WLA from accelerations recorded from the M5.7 Ocotillo event and the swarm of aftershocks.

Flexible to Rigid Casing Material Transfer Functions

Averages of the spectral amplitudes of the accelerations recorded in the 5.5m boreholes were also computed in the same way. The Discrete FFT of each component record was computed and smoothed with a 1% window. The amplitude spectra *for all 60 events >M3.0* were then averaged together.

Figure 10 below presents a summary of the results for the 5.5m borehole for each component. In this figure, the red line is the surface-to-downhole transfer function for the 5.5m borehole with the rigid casing. The green line is the surface-to-downhole transfer function for the 5.5m borehole with the flexible casing. The blue line is the ratio of the spectra of the flexible casing to the rigid casing. Thus the blue line represents the influence that the casing material may be having on the recorded signal.

The plots in this figure demonstrate that there are distinct similarities between the data collected by the accelerometers in the flexible and rigid casings. To investigate this further, we computed the standard deviations of the flexible to rigid spectral ratios (shown in Figure 11) and found that the in the north/south and east/west components of direction, the accelerometers did not show any significant difference within the 95% confidence range.

The vertical flexible-to-rigid spectral ratio is shown in Figure 12. The vertical component of acceleration had two frequency ranges with significant differences between the two types of casing materials. The first area where significant differences exist is between 15.2Hz and 18.0Hz with a mean ratio value of 0.623±0.126 at the 95% confidence range at 17.09 Hz. The second area where significant differences between the two vertical accelerations are seen is from 26.2Hz to 30.0Hz. Here the mean spectral ratio value is 1.953±0.297 at the 95% confidence level at 25.31Hz. We expect that these are the effects of tube waves in the casing material.
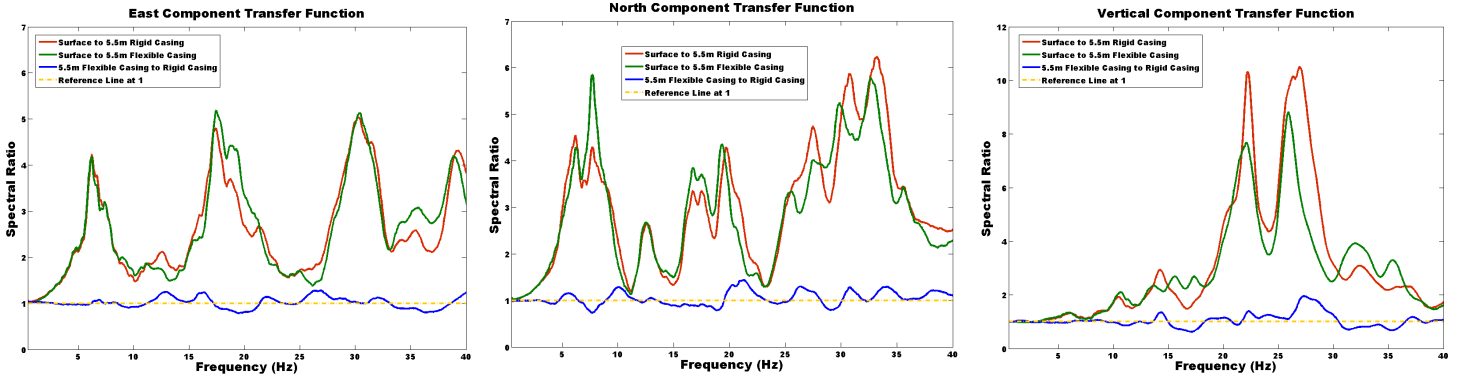
Figure 10. These plots are the average spectral ratios for the three components of motion. For each of the 60 events of magnitude greater than 3.0 (M > 3.0), the surface-to-downhole (5.5m) spectral ratio is computed for each component. These ratios are then averaged over all events. The red line is the average spectral ratio computed for the borehole with the rigid casing. The green line is the average spectral ratio computed for the borehole with the flexible casing. The blue line is the average spectral ratio computed between the borehole with the flexible casing and the borehole with the rigid casing.
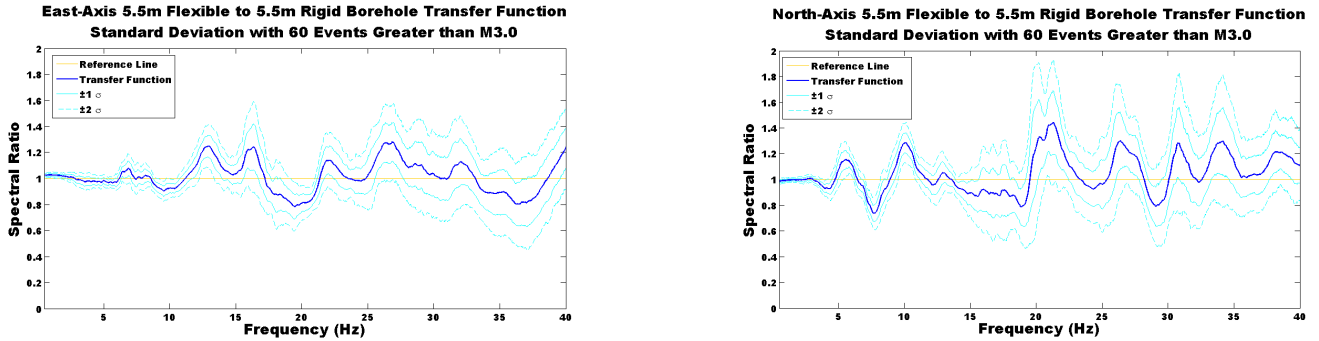
Figure 11. These plots show the mean, ±1σ, and ±2σ, of the 5.5m flexible to rigid spectral ratios for both horizontal components of motion. It is clear from these plots that within the 95% confidence range, changing the casing material did not have a significant influence on the recorded data.
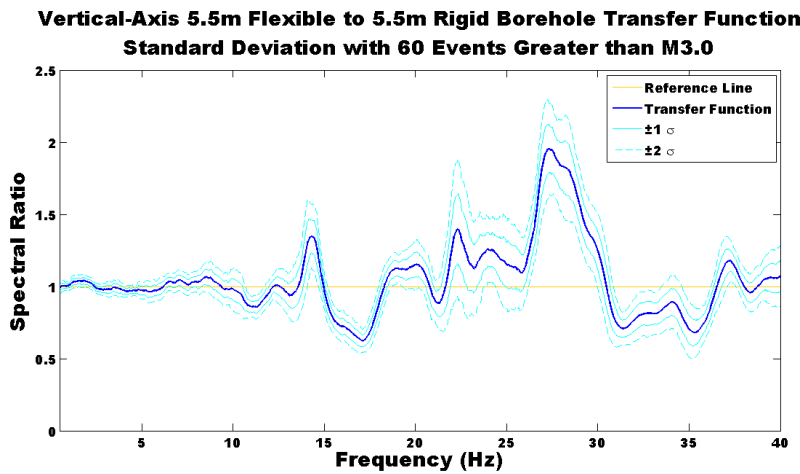

Figure 12. This plot shows the mean, ±1σ, and ±2σ, of the 5.5m flexible to rigid spectral ratio for the vertical component of acceleration. For this component, there appears to be a significant difference around 17 and 25 Hz.

CONCLUSIONS

We were fortunate to acquire the Ocotillo swarm, an ideal set of earthquakes approximately collocated with respect to the Wildlife Liquefaction Array. These data naturally lend themselves to a study of site effects, as comparisons can be made across the suite of events.

We find significant differences in the spectral ratios computed for 30m and 100m depths. In the horizontal components, the transfer functions to the surface show more peaks from 30m and have fewer peaks from 100m. This is most likely related to downgoing wave interference in the shallower data, as these waves have not been attenuated as much as in the deeper hole. The east and the north components also have different transfer functions, which suggest anisotropy or deviation from 1-D layered medium. Differences between the mainshock and aftershock spectral ratios suggests that nonlinear response may be starting to occur, even at these relatively moderate ground motion levels. The vertical-component transfer function is remarkably similar for all magnitudes of events.

This study will be enhanced further by the calculation of coherences between the surface and downhole data, which may be used to locate the destructive interference of downgoing waves on the borehole accelerations. We also want to compute theoretical transfer functions with a numerical model that can be compared to these data and examine both linear and nonlinear computational methods for computing the transfer function.

In 2004 when the instrumentation at WLA was upgraded, a new borehole at 5.5m was installed with a flexible casing adjacent to a borehole of the same depth with a conventional rigid casing. The goal of this experiment was to identify any artifacts in the records that may be induced by the casing material. The Ocotillo swarm was an ideal data set for testing this hypothesis. With these data, we have found that there is not a significant effect on the horizontal components of motion. The difference between spectral ratios in the vertical component seen between the two casings may be related to propagation of tube waves up the casing.

In the future, we would like to place another borehole, at the same 5.5m depth, adjacent to these two with no casing and an accelerometer installed directly into the material. The comparison of these records with the other two will help establish the influence of casing material on data collected from boreholes.

ACKNOWLEDGEMENTS

REFERENCES

Abercrombie, R. E. [1995], "Earthquake locations using single-station deep borehole recordings: Implications for microseismicity on the San Andreas fault in southern California", Jour. Geophys. Res., Vol. 100, No. B12, pp. 24,003-24,014.

Abercrombie, R. E. and P. Leary [1993], "Source Parameters of Small Earthquakes Recorded at 2.5km Depth, Cajon Pass, Southern California: Implications for Earthquake Scaling", Geophys. Res. Ltrs., Vol. 20, No. 14, pp. 1511 - 1514.

Bonilla, L. F., J. H. Steidl, J.-C. Gariel, and R. J. Archuleta [2002], "Borehole Response Studies at the Garner Valley Downhole Array, Southern California", Bull. Seism. Soc. Am., Vol. 92, No. 8, pp. 3165-3179.

Cox, B. R. [2006], "Development of a Direct Test Method for Dynamically Assessing the Liquefaction Resistance of Soils In Situ", Ph.D. Dissertation, The University of Texas at Austin.

Holzer, T. L., and T. L. Youd [2007], "Liquefaction, Ground Oscillation, and Soil Deformation at the Wildlife Array, California", Bull. Seism. Soc. Am., Vol. 97, No. 3, pp. 961-976.

Seale, S. H. and R. J. Archuleta [1989], "Site Amplification and Attenuation of Strong Ground Motion", Bull. Seism. Soc. Am., Vol. 79, No. 6, pp. 1673 – 1696.

Steidl, J. H., A. G. Tumarkin, and R. J. Archuleta [1996], "What is a Reference Site?", Bull. Seism. Soc. Am., Vol. 86, No. 6, pp. 1733 - 1748.

Steidl, J. H. [2000], "Site Response in Southern California for Probabilistic Seismic Hazard Analysis", Bull. Seism. Soc. Am., Vol. 90, No. 6B, pp. S149 – S169.

Steidl, J. H., and S. H. Seale [2010], "Observations and Analysis of Ground Motion and Pore Pressure at the NEES Instrumented Geotechnical Field Sites", *Proc. Fifth Intern. Conf. on Recent Adv. in Geo. Erthq. Engrg. and Soil Dyn.*, San Diego, CA, 1.33b.

Zeghal, M., and A.-W. Elgamal [1994]. "Analysis of Site Liquefaction Using Earthquake Records", Jour. Geotech. Engrg., Vol. 120, No. 6, pp. 996-1017.

Table 1: Earthquake Event Information

Events which are part of the dataset with Magnitude equal to or greater than 3.5 are shaded. Event numbers are for reference only.
A '*' indicates that the event was truncated because the following event occurred before the starred event ended

Event Number	Date (M/DD/YYYY)	Time (UTC)	Latitude	Longitude	Magnitude	Epicentral (km)	Depth (km)	Hypocentral (km)	Azimuth (°E of N)
Main Shock	6/15/10	4:26:56	32.700	-115.921	5.7	57.30	5.4	57.55	39.40
1	6/15/10	4:36:06	32.679	-115.924	4.1	59.29	12.5	60.60	38.17
2	6/15/10	4:40:36	32.665	-115.933	3.9	61.04	13.7	62.56	37.89
3	6/15/10	4:43:09	32.693	-115.947	3.7	59.46	12.4	60.74	40.72
4	6/15/10	4:46:04	32.724	-115.950	3.1	57.08	5.7	57.37	43.19
5	6/15/10	4:47:22	32.705	-115.935	3.5	57.72	5.7	58.00	40.75
6	6/15/10	4:56:47	32.705	-115.947	3.6	58.46	5.9	58.75	41.57
7*	6/15/10	4:59:04	32.680	-115.927	3.1	59.38	3.5	59.48	38.45
8	6/15/10	4:59:43	32.700	-115.950	4.6	59.06	10.7	60.02	41.42
9	6/15/10	5:08:43	32.641	-115.898	3.5	61.28	12.8	62.60	33.95
10*	6/15/10	5:30:58	32.668	-115.914	3.7	59.70	6.6	60.06	36.75
11	6/15/10	5:31:17	32.754	-115.989	3.7	57.36	1.6	57.38	48.11
12	6/15/10	5:34:14	32.709	-115.956	4.4	58.69	5.5	58.95	42.47
13	6/15/10	6:08:27	32.693	-115.951	3.8	59.71	14.2	61.37	40.99
14	6/15/10	6:23:35	32.689	-115.942	3.2	59.50	15.1	61.38	40.10
15	6/15/10	6:32:10	32.700	-115.916	3.5	57.00	14.1	58.72	39.04
16	6/15/10	6:40:17	32.697	-115.954	3.0	59.56	11.4	60.64	41.47
17	6/15/10	6:46:07	32.697	-115.923	3.6	57.68	12	58.91	39.33
18	6/15/10	6:52:25	32.682	-115.921	3.4	58.86	13.2	60.32	38.16
19	6/15/10	8:11:22	32.712	-115.947	3.6	57.88	0.5	57.88	42.08
20	6/15/10	8:14:45	32.688	-115.911	4.2	57.76	3.8	57.88	37.85
21	6/15/10	8:16:49	32.681	-115.913	4.0	58.49	5.6	58.75	37.52
22	6/15/10	8:26:45	32.671	-115.926	3.3	60.11	6.1	60.42	37.79
23	6/15/10	8:39:41	32.688	-115.927	3.1	58.69	4.5	58.86	38.99
24	6/15/10	8:56:59	32.677	-115.915	3.0	58.95	5.7	59.23	37.40
25	6/15/10	9:06:33	32.659	-115.908	3.1	60.17	6.2	60.49	35.75
26*	6/15/10	9:51:17	32.691	-115.930	3.6	58.61	5.3	58.85	39.41
27	6/15/10	9:52:18	32.699	-115.938	3.3	58.41	0.2	58.41	40.52
28	6/15/10	14:56:41	32.708	-115.957	3.3	58.83	3.5	58.94	42.46
29	6/15/10	16:32:30	32.709	-115.959	3.6	58.88	13.4	60.38	42.67
30	6/15/10	17:06:10	32.687	-115.906	3.7	57.56	13.5	59.12	37.41
31	6/15/10	21:36:36	32.704	-115.934	3.0	57.74	1.8	57.77	40.60
32	6/15/10	23:05:36	32.707	-115.974	3.1	60.00	7.2	60.43	43.50
33	6/15/10	23:30:46	32.725	-115.988	3.3	59.50	4.4	59.66	45.74

Event Number	Date (M/DD/YYYY)	Time (UTC)	Latitude	Longitude	Magnitude	Epicentral (km)	Depth (km)	Hypocentral (km)	Azimuth (°E of N)
34	6/16/10	2:42:01	32.667	-115.928	3.2	60.58	11.7	61.70	37.67
35	6/16/10	7:39:47	32.674	-115.921	3.3	59.56	0.2	59.56	37.63
36	6/16/10	10:04:43	32.628	-115.912	3.4	63.21	9.8	63.97	34.20
37	6/16/10	10:54:39	32.728	-115.974	3.6	58.33	3.4	58.43	45.08
38	6/16/10	11:30:46	32.696	-115.929	3.8	58.12	3.7	58.24	39.68
39	6/16/10	12:03:14	32.670	-115.929	3.0	60.37	0.2	60.37	37.93
40	6/16/10	15:09:11	32.677	-115.978	3.2	62.71	3	62.78	41.65
41	6/16/10	16:19:38	32.695	-115.940	3.2	58.87	1	58.87	40.38
42	6/16/10	17:53:25	32.711	-115.963	3.0	58.97	5.8	59.25	43.08
43	6/16/10	21:04:22	32.673	-115.897	3.4	58.31	4.1	58.45	35.83
44	6/16/10	21:21:47	32.670	-115.947	3.2	61.42	1.9	61.45	39.16
45	6/17/10	14:23:33	32.712	-115.977	3.3	59.79	3.4	59.89	44.06
46	6/18/10	13:57:23	32.700	-115.934	3.4	58.08	2.2	58.12	40.32
47	6/18/10	19:57:10	32.719	-115.972	3.0	58.91	0	58.91	44.27
48	6/18/10	23:02:09	32.683	-115.924	3.0	58.95	5.8	59.23	38.44
49	6/21/10	12:26:17	32.730	-115.993	3.1	59.45	1.9	59.48	46.43
50	6/24/10	17:07:34	32.720	-115.963	4.0	58.24	1.2	58.26	43.75
51	6/25/10	0:10:32	32.718	-115.967	3.1	58.66	1.7	58.69	43.87
52	6/26/10	23:55:55	32.698	-115.918	3.0	57.29	3.2	57.38	39.04
53	6/27/10	0:17:42	32.672	-115.919	3.3	59.62	7.9	60.14	37.36
54	6/28/10	3:39:30	32.714	-115.950	3.1	57.90	1.2	57.91	42.44
55	6/30/10	8:03:02	32.665	-115.912	3.6	59.85	12.6	61.16	36.41
56	7/3/10	4:30:16	32.736	-115.976	3.0	57.84	5	58.05	45.84
57	7/11/10	14:32:51	32.670	-115.869	3.1	57.09	8.1	57.66	33.52
58	7/12/10	21:10:12	32.670	-115.919	3.2	59.80	12.1	61.01	37.23
59	7/24/10	2:29:41	32.726	-115.979	4.0	58.81	3.5	58.91	45.39
60	8/8/10	16:41:33	32.725	-115.977	3.5	58.76	3.1	58.84	45.04